J. Fluid Mech. (1972), *vol.* 53, part 1, *pp.* 113-127
Printed in Great Britain

Turbulent hypersonic flow at a wedge-compression corner

By G. M. ELFSTROM
Department of Aeronautics, Imperial College, London?

(Received 25 October 1971)

A hypersonic gun tunnel has been used to investigate turbulent shock-boundary-layer interaction at a wedge-compression corner. The results extend the Mach number range of existing data, in particular of incipient separation.

1. Introduction

Interactions between oblique shock waves and boundary layers must be properly understood for adequate prediction of the performance of various aerodynamic devices used on hypersonic cruising vehicles, e.g. flaps, spoilers and inlets. This paper is concerned with the special case of turbulent shock-boundary-layer interaction at a two-dimensional wedge-compression corner. Prediction methods tend to be semi-empirical, with the exception of the Todisco & Reeves (1969) strong interaction theory, and earlier experimental studies have been conducted at supersonic Mach numbers over limited Reynolds number ranges, e.g. Kuehn (1959), Thomke & Roshko (1969). The experiments described here were undertaken to extend the Mach number range of existing data, with emphasis on identifying the incipient separation condition.

2. Apparatus

All tests were carried out in the Imperial College no. 2 hypersonic gun tunnel. A full account of the design and operation of this facility was given by Needham, Elfstrom & Stollery (1970). Briefly, it consists of a free-piston compression heater feeding a hypersonic blow-down tunnel. A fully contoured nozzle provides a Mach 9 nitrogen gas open-jet test flow. At the normal driving pressure of 1000 atm, the running time is about 25ms. For all the tests described here a reservoir temperature of 1070 °K was used.

The model used was a sharp flat plate plus a trailing flap instrumented for pressure measurements. Overall, the model was 43 cm to the hinge line, 17·8 cm wide, with a 10 cm chord full-span flap. Figure 1 shows the model in relation to the working section. Pressure tappings at 2·54 mm intervals along the model centre-line were connected to unbonded strain-gauge transducers; an electric resistance element embedded in the model heated the wall to temperatures T_w in the range 295 °K $\leqslant T_w \leqslant$ 770 °K with a variation of $\pm$ 10 °K over the surface.

† Present address: University of Tennessee Space Institute, Tullahoma.

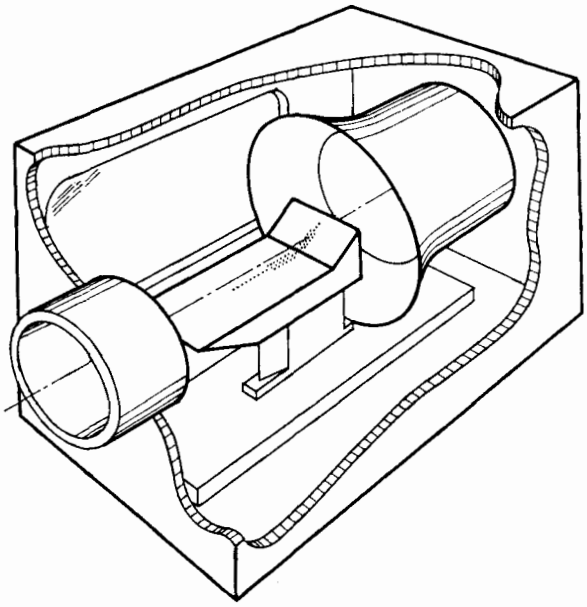

FIGURE 1. Pictorial view of model in gun tunnel working section.

Local Mach numbers of 7 and 8 were obtained by inclining the model to the Mach 9 test flow.

3. Results and discussion

With the exception of the Mach 7 and 8 data, all the results have been tabulated by Elfstrom (1971). Only a summary is presented here.

Pitot pressure profiles were completed using a Pitot rake assembly to check that the boundary layer was turbulent ahead of the hinge line. The Rayleigh Pitot formula was used along with the usual assumption of constant static pressure across the boundary layer to calculate Mach number profiles. A Pitot displacement correction of $0{\cdot}15d$, where d is the thickness of the flattened probe, was applied to all points. Velocity profiles were then calculated as described below, using the linear Crocco temperature–velocity relation

$$\frac{T}{T_\infty} = 1 + r\frac{\gamma-1}{2}M_\infty^2\left[1-\left(\frac{u}{u_\infty}\right)^2\right] + \frac{T_w - T_r}{T_\infty}\left(1-\frac{u}{u_\infty}\right), \tag{1}$$

where

$$\frac{T_r}{T_\infty} = 1 + r\frac{\gamma-1}{2}M_\infty^2, \tag{2}$$

$r = 0{\cdot}9$, T is temperature, u velocity in the x direction (x being distance from the leading edge along the surface), M the Mach number and the subscripts ∞, r and w refer to free-stream or undisturbed conditions, adiabatic wall conditions and conditions at the wall respectively. The substitution

$$\frac{u}{u_\infty} = \frac{M}{M_\infty}\frac{a}{a_\infty} = \frac{M}{M_\infty}\left(\frac{T_\infty}{T}\right)^{\frac{1}{2}} \tag{3}$$

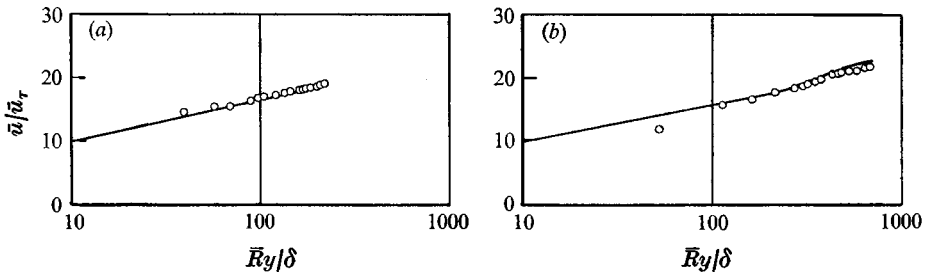

FIGURE 2. Flat-plate velocity profiles in equivalent incompressible co-ordinates. ○, experiment; —, Coles's law of wall and wake. (*a*) $M_\infty = 8{\cdot}96$, $\bar{R} = 220$, $T_w = 0{\cdot}3T_r$ ($\bar{\pi} = 0$). (*b*) $M_\infty = 9{\cdot}22$, $\bar{R} = 680$, $T_w = 0{\cdot}3T_r$ ($\bar{\pi} = 0{\cdot}4$).

was made in the Crocco relation and resulted in a quadratic equation solvable for $(T/T_\infty)^{\frac{1}{2}}$. The solution was then substituted into (3) to find u/u_∞. Hopkins, Keener & Dwyer (1971) found that the Van Driest (1951) function

$$\frac{\bar{u}}{\bar{u}_\tau} = \frac{1}{D[\frac{1}{2}C_{f\infty}T_w/T_\infty]^{\frac{1}{2}}}\left\{\sin^{-1}\left[\frac{2D^2u/u_\infty - E}{(E^2+4D^2)^{\frac{1}{2}}}\right] + \sin^{-1}\left[\frac{E}{(E^2+4D^2)^{\frac{1}{2}}}\right]\right\}, \tag{4}$$

where $$D = \left(0{\cdot}2M_\infty^2\frac{T_\infty}{T_w}\right)^{\frac{1}{2}}, \quad E = \frac{T_\infty}{T_w} + D^2 - 1,$$

$\bar{u}_\tau$ is the friction velocity and C_f is the skin friction coefficient, yielded the best transformation of non-adiabatic wall velocity profiles to equivalent incompressible values. This transformation was applied to the present profiles, with results as shown in figure 2. The values of $C_{f\infty}$ used were derived from the heat-transfer rate measurements made in the gun tunnel by Coleman, Elfstrom & Stollery (1971) using a Reynolds analogy factor ($2St/C_{f\infty}$) of 1·16, where St is the Stanton number. Also shown in figure 2 is Coles's (1962) law of the wall and wake

$$\frac{\bar{u}}{\bar{u}_\tau} = \frac{1}{K_i}\ln\bar{R}\frac{y}{\delta} + B_i + \frac{\bar{\pi}}{K_i}\omega\left(\frac{y}{\delta}\right), \tag{5}$$

where $K_i = 0{\cdot}41$, $B_i = 5{\cdot}0$, $\bar{R}$ is the Reynolds number based on conditions at the wall, δ is the boundary-layer thickness, $\bar{\pi}$ is the amplitude of the wake component in velocity profile, y is the distance normal to the surface and ω, the wake function recommended by Alber & Coats (1969), is given by

$$\omega(y/\delta) = 1 - \cos(\pi y/\delta). \tag{6}$$

The values of $\bar{\pi}$ shown in the figure were taken from the $\bar{\pi}$ *vs.* $\bar{R}$ tabulation given by Coles. Measurements near the wall were undoubtedly subject to wall–Pitot interference effects.

Static pressure distributions at various flap angles under conditions of constant $M_\infty, Re_{\delta_L}, T_0$ (the reservoir temperature) and T_w are shown in figure 3. It can be seen that for attached flow (wedge angle $\alpha \leqslant 30°$) the upstream influence is limited to much less than one boundary-layer thickness. The final pressure on the wedge is always close to the inviscid level, i.e. that for a flow at M_∞ turning through an angle α via a single shock. For angles greater than 30° the upstream influence increases with α and rapidly develops a plateau of increasing length,

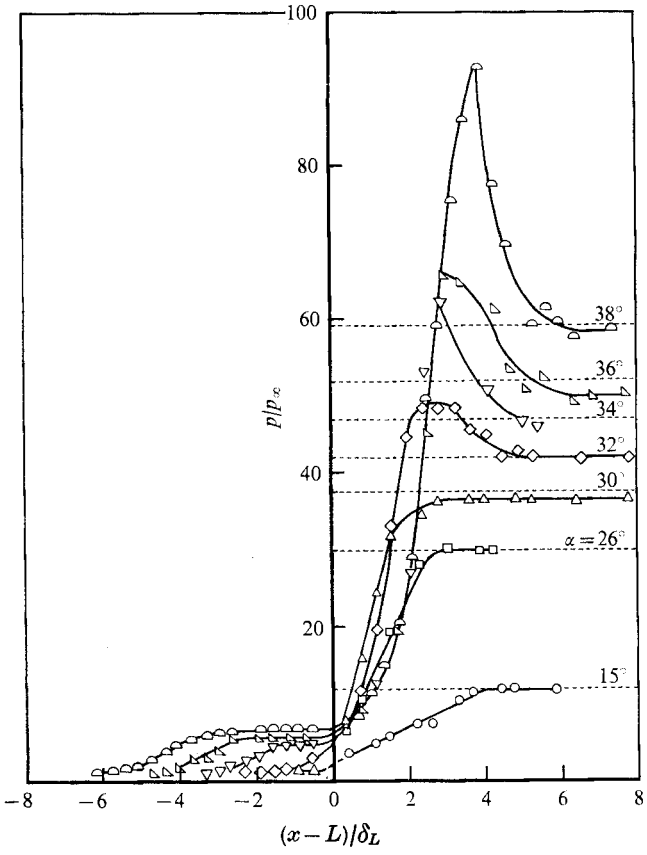

FIGURE 3. Static pressure distributions at a wedge-compression corner, L being the length of the flat plate to the hinge line. – – –, inviscid distribution. Experiment: $M_\infty = 9{\cdot}22$, $Re_{\delta L} = 4 \times 10^5$, $T_0 = 1070$ °K, $T_w = 295$ °K.

	⌓	◺	▽	◇	△	□	○
α	38°	36°	34°	32°	30°	26°	15°

indicative of separated flow. Associated with this is the formation of a pressure overshoot on the wedge.

3.1. *Attached flow*

Figure 4 shows that the effect of a change in either Reynolds number of wall temperature on an attached flow pressure distribution is essentially negligible. This is to be expected because the incoming velocity profiles are similar. The upstream influence is very small, indicating a thin subsonic region in the approaching boundary layer. Schlieren photographs show that the oblique shock wave penetrates deep into the boundary layer, almost to the corner. Thomke & Roshko (1969) made similar observations in their experiments and on this basis developed a method of characteristics to predict the static pressure distribution on the wedge in attached flow. In an effort to reduce the complexity of the calculations, the following simplified model was developed. The input Mach number profile is obtained from Coles's law of the wall and wake by using the Van Driest transformation and the Crocco linear temperature–velocity relation as outlined

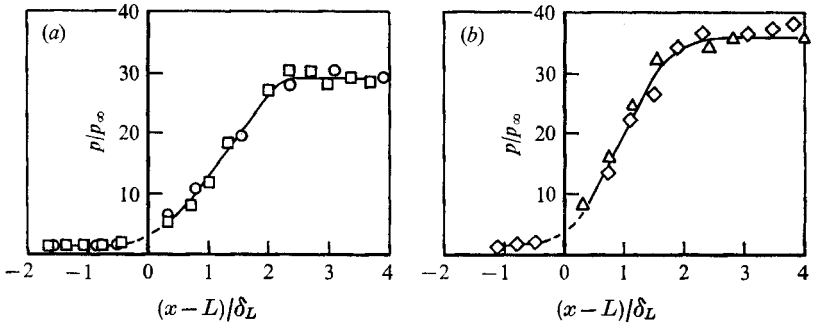

FIGURE 4. Attached flow static pressure distributions. (*a*) Effect of wall temperature. $M_\infty = 9{\cdot}22$, $Re_{\delta_L} \simeq 4\times10^5$, $\alpha = 26°$. ○, $T_w = 0{\cdot}3T_r$; □, $T_w = 0{\cdot}68T_r$. (*b*) Effect of Reynolds number. $M_\infty \simeq 9$, $T_w = 0{\cdot}3T_r$, $\alpha = 30°$. ◇, $Re_{\delta_L} = 1\times10^5$; △, $Re_{\delta_L} = 4\times10^5$.

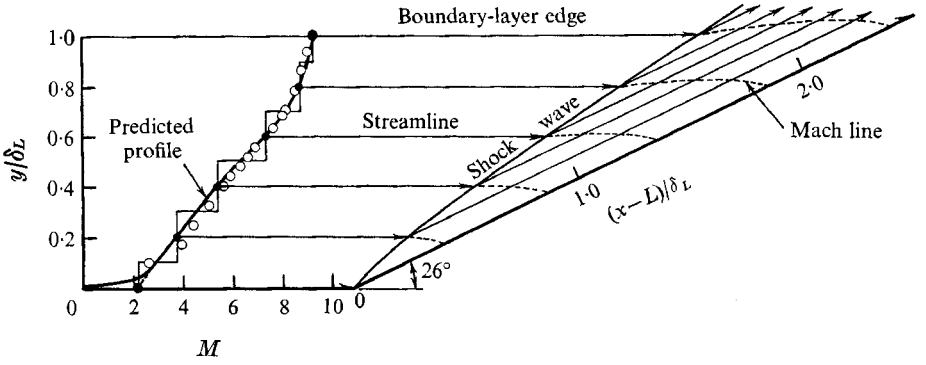

FIGURE 5. Example of the construction of an attached flow field at a wedge-compression corner. ○, experiment, $M_\infty = 9{\cdot}22$, $Re_{\delta_L} = 4\times10^5$, $T_w = 0{\cdot}3T_r$; ●, Mach numbers used in computation.

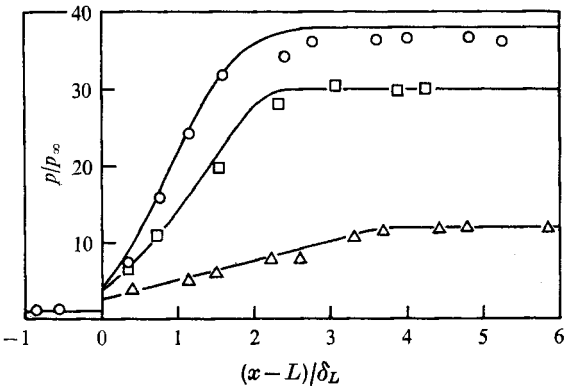

FIGURE 6. Prediction of attached flow static pressure distribution at a wedge-compression corner. —, present theory. Experiment: $M_\infty = 9{\cdot}22$, $Re_{\delta_L} = 4\times10^5$, $T_w = 0{\cdot}3T_r$; ○, $\alpha = 30°$; □, $\alpha = 26°$; △, $\alpha = 15°$.

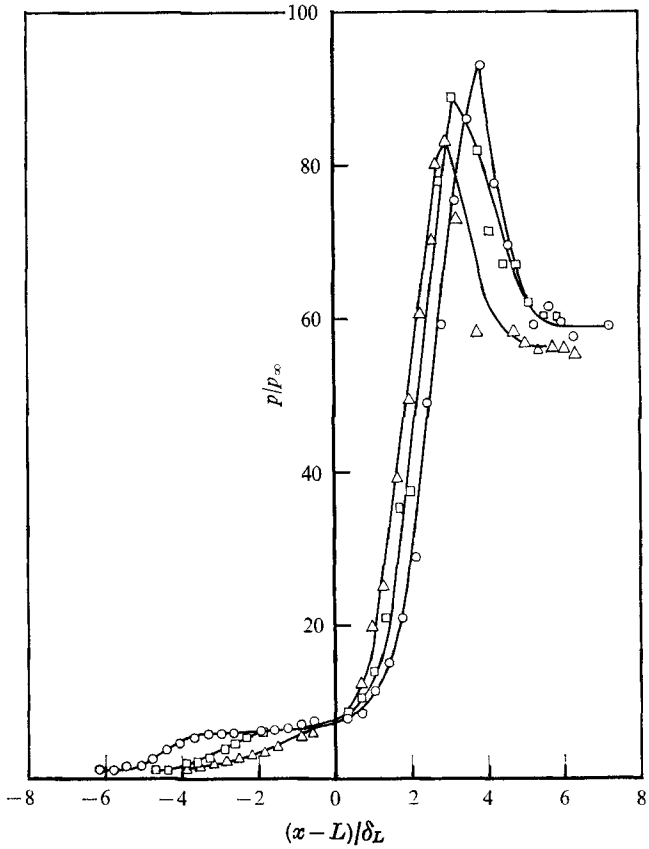

FIGURE 7. Effect of Reynolds number on a separated flow static pressure distribution. $M_\infty \simeq 9, T_w = 0{\cdot}3T_r, \alpha = 38°$; △, $Re_{\delta_L} = 1\times10^5$; □, $Re_{\delta_L} = 2\times10^5$; ○, $Re_{\delta_L} = 4\times10^5$.

in equations (1)–(6). The viscous subsonic layer is ignored on the assumption that it is very thin. An extrapolation of the linear portion of the Mach number profile produces a 'wall' or 'slip' Mach number at the surface. For computational purposes, the incoming boundary layer is stratified into independent streams as shown in figure 5. Although six layers are shown, in fact, twelve layers were used. The entire flow is assumed to pass through an oblique shock and to turn parallel to the wall. Further, the pressure disturbances are assumed to travel to the surface via Mach lines, and do not reflect. This behaviour is not strictly correct because only the layer next to the wall will turn parallel to the wall in going through the shock; other layers will turn through a slightly smaller angle. Also, the pressure disturbances will reflect from the wall. However, as far as the wall static pressure distribution is concerned, these effects tend to cancel. Computation is begun at the wall and proceeds to $y = \delta_L$, the boundary-layer thickness at the hinge. The Mach number at the centre of each layer is used in the calculation of that segment of the oblique shock and other flow properties. Examples of the resulting pressure distribution are shown in figure 6. The good agreement between theory and experiment, though perhaps fortuitous, shows that the simple model can provide reasonable estimates of attached flow static pressure distributions.

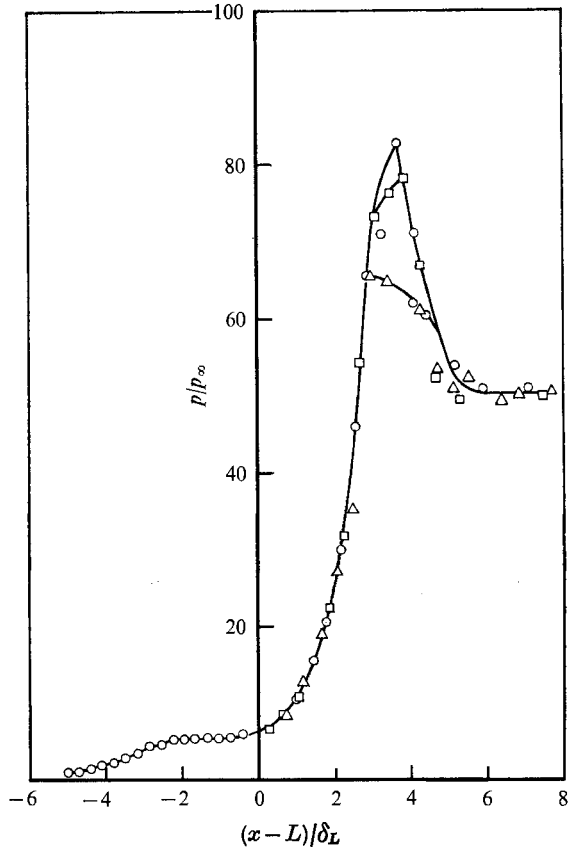

FIGURE 8. Effect of wall temperature on a separated flow static pressure distribution. $M_\infty = 9{\cdot}22$, $Re_{\delta_L} \simeq 4\times10^5$, $\alpha = 36°$. △, $T_w = 0{\cdot}3T_r$; □, $T_w = 0{\cdot}49T_r$; ○, $T_w = 0{\cdot}68T_r$.

3.2. *Separated flow*

Raising the Reynolds number in separated flow consistently increased both the extent of separation and the magnitude of the pressure overshoot, as seen in figure 7. The plateau pressure, however appears to be independent of the Reynolds number. Kuehn (1959) found similar trends with a Reynolds number Re_{δ_L} based on δ_L, while Thomke & Roshko (1969) found opposite trends. Since these two sets of data are separated by at least an order of magnitude in Re_{δ_L}, there may be a reversal in the trend with Re_{δ_L}. Only further experiments will verify this. The effect of an increase in the wall temperature ratio T_w/T_r appears almost negligible in well-separated flow, as seen in figure 8. It should be noted, however, that the magnitude of the pressure overshoot increases with T_w/T_r. When close to incipient separation, the effect of an increase in T_w/T_r is small but adverse, i.e. raising the wall temperature promotes an earlier separation. Figure 9 shows the effect of wall temperature on pressure distributions ahead of the corner. Reducing the free-stream Mach number increases the extent of the separated region and decreases the plateau pressure, as shown in figure 10. These trends are consistent with those found by Kuehn (1959) and Thomke & Roshko (1969).

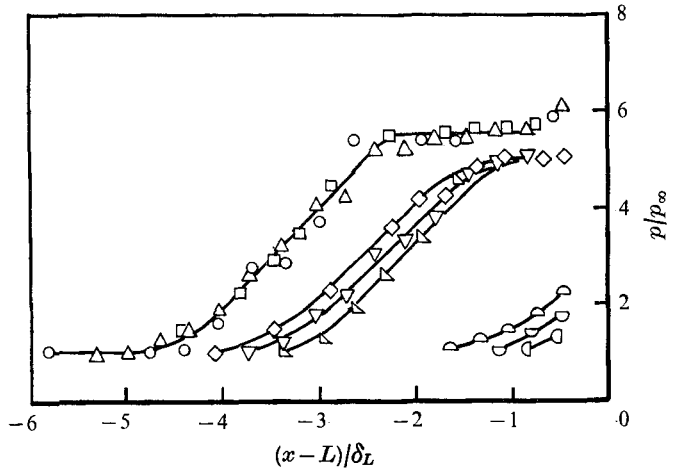

FIGURE 9. Effect of wall temperature on pressure distributions ahead of the corner. $M_\infty = 9{\cdot}22$, $Re_{\delta_L} \simeq 4 \times 10^5$.

	○	△	□	▷	▽	◇	◁	▽	▷
α	36°	36°	36°	34°	34°	34°	30°	30°	30°
T_w/T_r	0·3	0·49	0·68	0·3	0·49	0·68	0·3	0·49	0·68

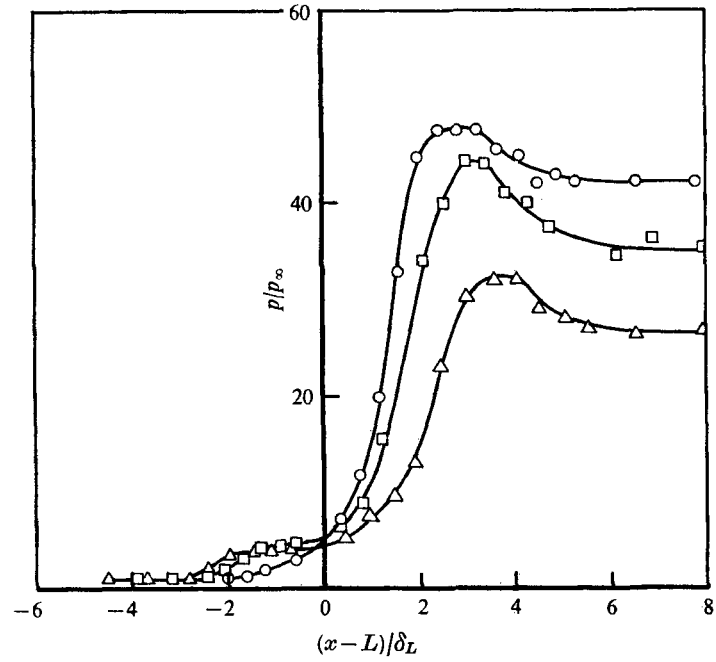

FIGURE 10. Effect of Mach number on a separated flow static pressure distribution. $Re_{\delta_L} \simeq 4 \times 10^5$, $T_w = 0{\cdot}3T_r$. ○, $M_\infty = 9{\cdot}22$; □, $M_\infty = 8{\cdot}2$; △, $M_\infty = 7{\cdot}3$.

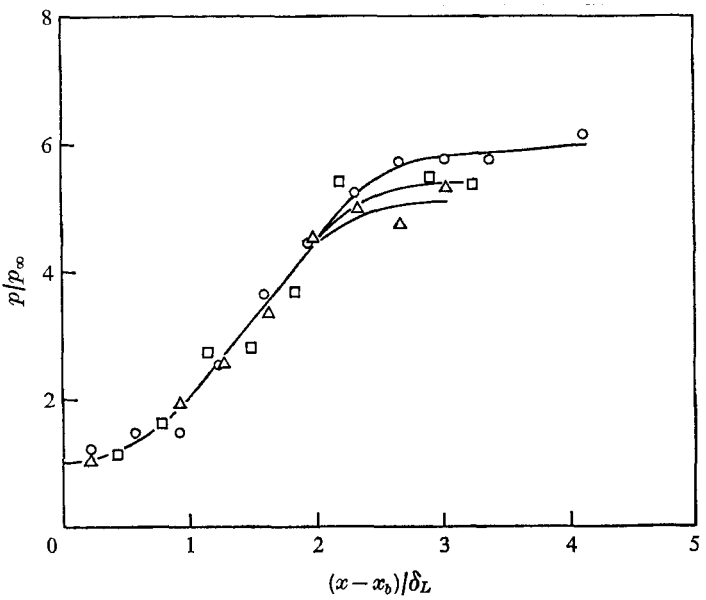

FIGURE 11. Pressure distributions at separation. x_b is the value of x at the beginning of an interaction in separated flow. $M_\infty = 9{\cdot}22$, $Re_{\delta_L} = 4\times10^5$, $T_w = 0{\cdot}3T_r$. ○, $\alpha = 38°$; □, $\alpha = 36°$; △, $\alpha = 34°$.

The free interaction concepts proposed by Chapman, Kuehn & Larsen (1958) indicate that the pressure rise to separation is independent of the agency provoking the separation, in this case the wedge angle. A simple test of this concept is shown in figure 11. The pressure distributions near separation (at constant free-stream conditions) are matched at the beginning of the pressure rise. The figure shows that the pressure distributions collapse onto one curve up to separation, while the final pressure appears to be a function of the wedge angle, a behaviour similar to that found by Chapman *et al.* (1958) in their own experiments.

The theories of Reshotko & Tucker (1955) and Todisco & Reeves (1969) assumed that the plateau pressure p_p was independent of the final downstream conditions. Their predictions are shown in figure 12(*a*) along with a collection of data at a wedge-compression corner. Included is a data point from the preliminary study of Appels & Backx (1971). The data do not agree well with either theory and, as mentioned above, the present results show p_p/p_∞ to be a function of α. A simple scaling p_p/p_{INV} was applied to the data, where p_{INV} is the inviscid pressure the flow would attain if it were attached. Figure 12(*b*) is a convincing demonstration that the final downstream pressure controls the plateau pressure. Only further experiment will show whether the scaling is a linear one.

A consistent feature of the present results is the appearance of an overshoot pressure in separated flow. This phenomenon is probably due to the intersection of the separation and reattachment shock waves close to the surface. Sullivan (1963) examined the inviscid flow field associated with the intersection of the two shocks arising from a double wedge. He showed that in hypersonic flow the intersection would result in a strong expansion wave if the second turning angle

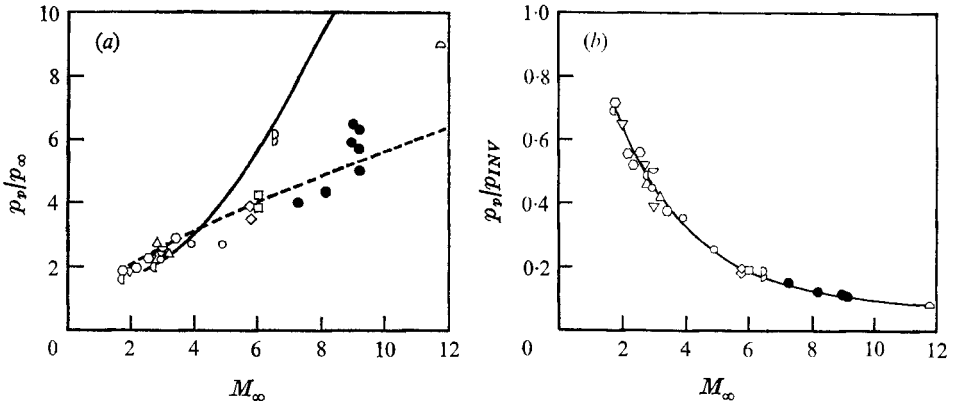

FIGURE 12. Correlations of plateau pressure ahead of a wedge-compression corner. Theory: —, Todisco & Reeves (1969); – – –, Reshotko & Tucker (1955). Experiment: ⌓, Appels & Backx (1971); ⌔, Bogdonoff & Kepler (1955); ▽, Chapman *et al.* (1958); ◖, Drougge (1953); □, Gray & Rhudy (1971); △, Kessler *et al.* (1970); ⟨⟩, Kuehn (1959); ◇, Sterrett & Emery (1962); ○, Thomke & Roshko (1969); ▷, Todisco & Reeves (1969); ●, present study.

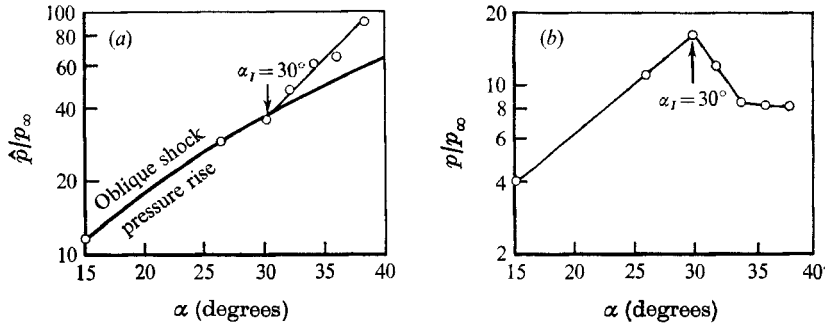

FIGURE 13. Detection of incipient separation at a wedge-compression corner.

$$M_\infty = 9{\cdot}22,\ Re_{\delta_L} = 4\times 10^5,\ T_w = 0{\cdot}3T_r.$$

(*a*) Disappearance of pressure overshoot ($\hat{p}$ = peak or overshoot pressure). (*b*) p/p_∞ at $(x-L)/\delta_L = 0{\cdot}77$.

was greater than the first. Hence the static pressure at the surface could reach a very high value behind the second shock and then drop rapidly to a value close to p_{INV}. This indeed closely describes the pressure distributions on the wedge in separated flow. In this context it is interesting to note that Gray & Rhudy (1971) found strong pressure overshoots at $M_\infty = 6{\cdot}05$. Also, the data of Thomke & Roshko (1969) exhibits slight overshoots at $M_\infty = 3{\cdot}93$. It thus appears that pressure overshoots are primarily a hypersonic phenomenon.

3.3. *Incipient separation*

Kuehn (1959) associated the incipient separation condition with the appearance of a kink in the pressure distribution near the corner. This criterion was not applied to the present results as it requires pressure distributions over a series of very closely spaced wedge angles.

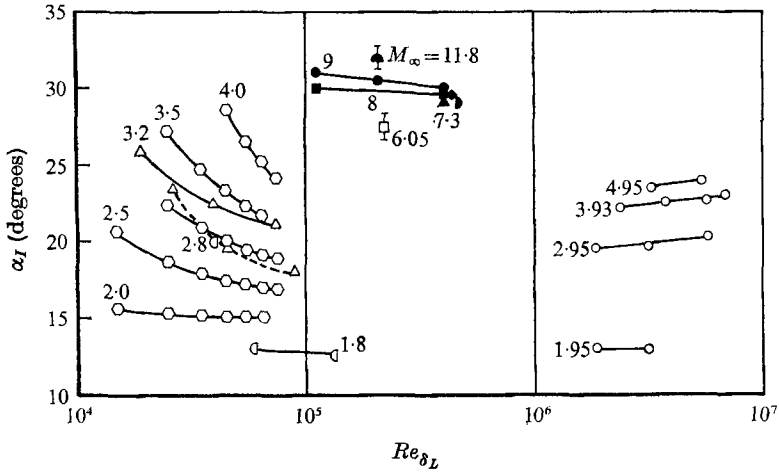

FIGURE 14. Incipient separation at a wedge-compression corner. ◓, Appels & Backx (1971), $T_w = 0{\cdot}13T_r$; ▲, ■, ●, present study, $T_w = 0{\cdot}3T_r$; ◆, present study, $T_w = 0{\cdot}49T_r$; ◗, present study, $T_w = 0.68T_r$; □, Gray & Rhudy (1971), $T_w = T_r$; △, Kessler *et al.* (1970), $T_w = T_r$; ⬭, Kuehn (1959), $T_w = T_r$; ○, Thomke & Roshko (1969), $T_w = T_r$.

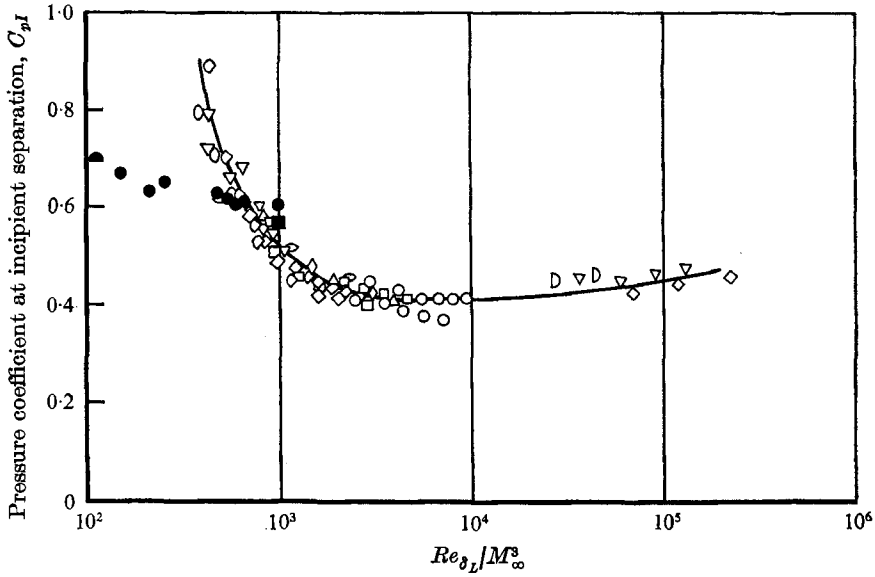

FIGURE 15. Incipient separation correlation of Kessler *et al.* (1970). Open symbols, data presented in figure 37 of Kessler *et al.* (1970). ◓, Appels & Backx (1971), $M_\infty = 11{\cdot}8$; ●, present study $7.3 \leqslant M_\infty \leqslant 9{\cdot}22$; ■, Gray & Rhudy (1971), $M_\infty = 6{\cdot}05$.

Disappearance of the pressure overshoot appears to be a promising criterion for detection of incipient separation at hypersonic speeds. An example of this is shown in figure 13(*a*) and agrees quite well with the Thomke & Roshko (1969) criterion (figure 13(*b*)), which associates incipient separation with a break in the pressure variation with α at some point on the wedge. The accuracy of these methods is estimated to be $\pm 0{\cdot}5°$.

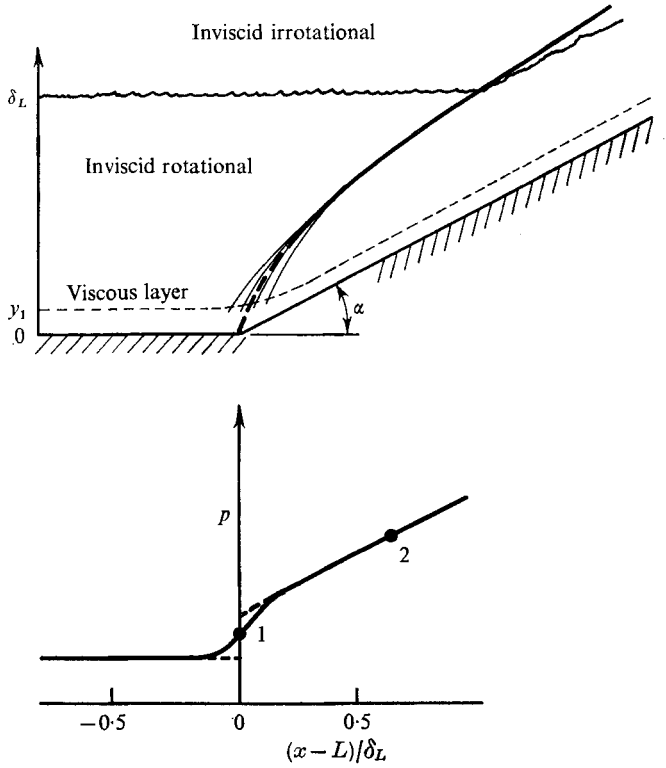

FIGURE 16. Three-layer model of an attached flow field at a wedge-compression corner. – – –, oblique shock trajectory in two-layer model; —, oblique shock trajectory in three-layer model; – – –, edge of laminar layer.

A collection of incipient separation data for supersonic turbulent flow at a wedge-compression corner is given in figure 14. Drougge (1953) did not identify α_I, the wedge angle at incipient separation, in his results, so the 'kink' criterion of Kuehn was applied. The 'overshoot' criterion described above was applied to Gray & Rhudy's data to obtain the point shown. The present results follow the trends found by Kuehn (1959) and Kessler, Reilly & Mockapetris (1970) but with a much weaker dependent on Re_{δ_L}. Also, the trends with T_w/T_r are quite small. Kessler *et al.* produced a correlation which took into account the reversed trends found by Thomke & Roshko. In figure 15 the present results and other recent data have been added to the collection of Kessler *et al.* It appears that their correlation severely overpredicts the trends with Re_{δ_L} at high M_∞.

In the present experiments it was observed that at incipient separation the oblique shock wave penetrated the turbulent boundary layer almost to the wall, and the static pressure distribution appeared similar to those at lower wedge angles. Thus it would be reasonable to conclude that the mechanism of incipient separation is confined to a very small subsonic region at the corner. This point can be pursued further. The simple two-layer model of the attached flow field (as described in § 3.1) can be modified to include the presence of a laminar sublayer at the wall, as seen in figure 16 (the sonic line is not shown). The pressure distribution in region 2 is assumed to be largely controlled by reflexions from the

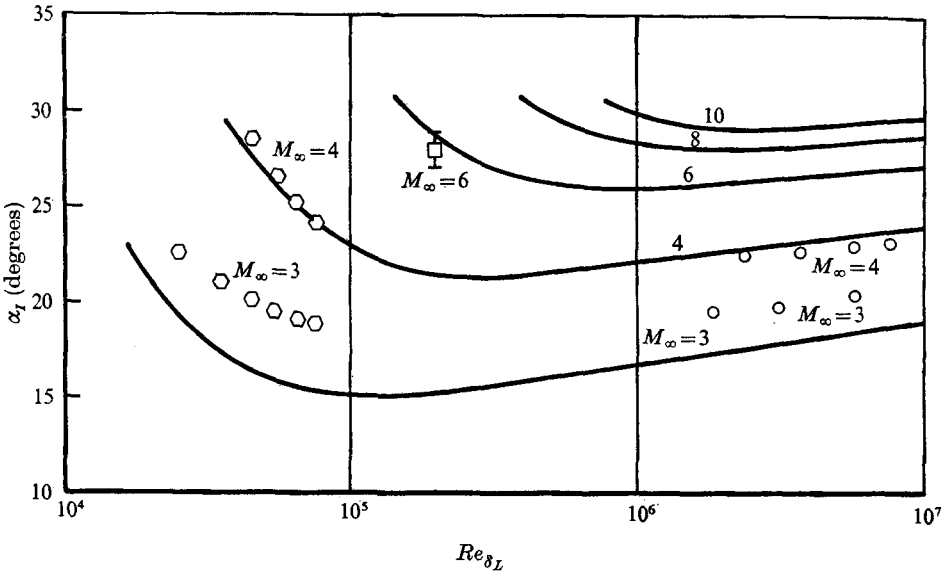

FIGURE 17. Estimation of incipient separation for adiabatic wall conditions. —, prediction using two-layer model. Experiment: ⬭, Kuehn (1959); □, Gray & Rhudy (1971); ○, Thomke & Roshko (1969).

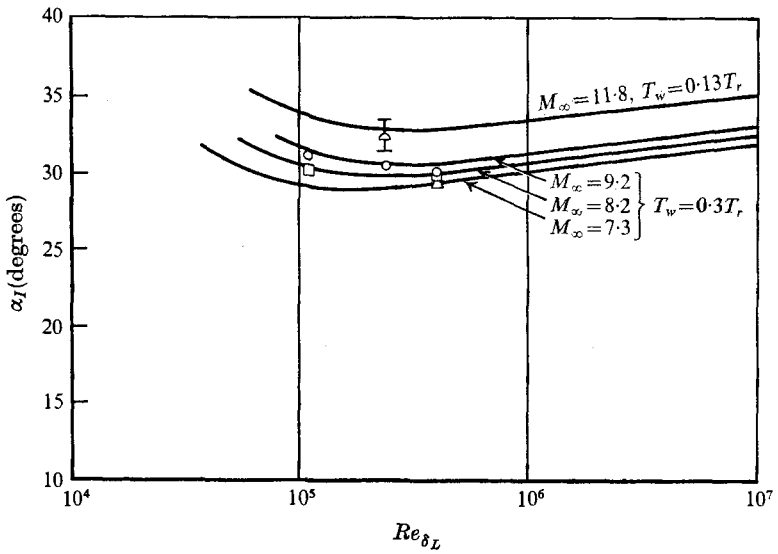

FIGURE 18. Estimations of incipient separation for non-adiabatic wall conditions. —, prediction using two-layer model; Experiment: ⬭, Appels & Backx (1971), $M_\infty = 11{\cdot}8$, $T_w = 0{\cdot}13T_r$; ○, present study, $M_\infty \simeq 9$, $T_w = 0{\cdot}3T_r$; □, present study, $M_\infty = 8{\cdot}2$, $T_w = 0{\cdot}3T_r$; △, present study, $M_\infty = 7{\cdot}3$, $T_w = 0{\cdot}3T_r$.

oblique shock wave in the turbulent layer, while that in region 1 is determined by a strong interaction between the laminar sublayer and the shock wave. Because, in general, laminar boundary layers separate when they encounter a normal shock wave, it would seem reasonable to guess that the maximum wedge angle possible at incipient separation would be that at which the simple

two-layer model would predict a normal shock wave at the wall. Figures 17 and 18 compare these estimates with experiment. The predicted values generally appear to be above the experimental results but are quite good except at low Mach numbers.

The analysis presented here is largely based on conjecture; the good agreement between experiment and theory at higher Mach numbers may be coincidental. However, an interesting feature of the predictions is worth discussing. The reversal in the α_I trend with Re_{δ_L} is due entirely to the development of the wake component in the turbulent velocity profile; if the wake component $\bar{\pi}$ were either zero or a constant, α_I would always increase with Re_{δ_L}. This may explain the reversed trends of Thomke & Roshko's data compared with Kuehn's data.

The high M_∞, high Re_{δ_L} test of the prediction has yet to be made. Further, there does not appear to be any data with which to test the input boundary-layer profile predictions at high M_∞ and Re_{δ_L}. Until such data are obtained, the fundamental parts of the flow model remain in doubt. The good agreement with the present experiments in terms of Mach number profiles and α_I trends is nonetheless encouraging, and suggests that the model can supply at least a reasonable estimate for the upper limit to α_I prediction at hypersonic Mach numbers.

4. Conclusions

Experiments have been carried out which extend the Mach number range of existing turbulent shock-boundary-layer interaction data. A simple method for predicting attached flow pressure distributions at a wedge-compression corner is presented and a simple analysis which helps to explain the observed trends of incipient separation with Mach number and Reynolds number is also given.

The author wishes to thank his supervisor Mr J. L. Stollery for his excellent guidance and support through this work. The research was sponsored in part by the Ministry of Aviation Supply under contract AT/2037/057. The author also wishes to thank the U.K. Department of Trade and Industry, and the National Research Council of Canada for their sponsorship in the form of an Athlone Fellowship and an NRC post-graduate scholarship, respectively.

REFERENCES

Alber, E. I. & Coats, D. E. 1969 *A.I.A.A. Paper*, no. 69–689.

Appels, C. & Backx, E. 1971 *V.K.I. Rep.* (unpublished).

Bogdonoff, S. M. & Kepler, C. E. 1955 *J. Aero. Sci.* **22**, 414–424.

Chapman, D. R., Kuehn, D. M. & Larsen, H. K. 1958 *N.A.C.A. Rep.* no. 1356.

Coleman, G. T., Elfstrom, G. M. & Stollery, J. L. 1971 *A.G.A.R.D. Symposium on Turbulent Shear Flows, London, Paper*, no. 31.

Coles, D. E. 1962 *Rand. Corp. Rep. R*-403-*PR.*

Drougge, G. 1953 *F.F.A. Rep. Sweden*, no. 47.

Elfstrom, G. M. 1971 Ph.D. thesis, University of London. (See also *Imperial College. Aero Rep.* 71–16.)

Gray, J. D. & Rhudy, R. W. 1971 *AEDC*-Tr-70-235.

HOPKINS, E. J., KEENER, E. R. & DWYER, H. A. 1971 *A.I.A.A. Paper*, no. 71–167.

KESSLER, W. C., REILLY, J. F. & MOCKAPETRIS, L. J. 1970 *McDonnell Douglas Corp. Rep.* MDCE 0264.

KUEHN, D. M. 1959 *N.A.S.A. Memo*, 1-21-59A.

NEEDHAM, D. A., ELFSTROM, G. M. & STOLLERY, J. L. 1970 *Imperial College. Aero Rep.* 70-04.

RESHOTKO, E. & TUCKER, M. 1955 *N.A.C.A. Tech. Note*, no. 3454.

STERRETT, J. R. & EMERY, J. C. 1962 *N.A.S.A. Tech. Note*, D-1014.

SULLIVAN, P. A. 1963 *A.I.A.A. J.* **1**, 1927.

THOMKE, G. J. & ROSHKO, A. 1969 *McDonnell Douglas Co. Rep.* D.A.C. 59819.

TODISCO, A. & REEVES, B. L. 1969 *Paper presented at the Symposium on Viscous Interaction Phenomena in Supersonic and Hypersonic Flow.* Wright-Patt. AFB.

VAN DRIEST, E. R. 1951 *J. Aero. Sci.* **18**, 145–160.